IEICE TRANS. ELECTRON., VOL.E107–C, NO.5 MAY 2024

PAPER

Simplified Reactive Torque Model Predictive Control of Induction Motor with Common Mode Voltage Suppression

Siyao CHU[†], **Bin WANG**[†a)], ***and*** **Xinwei NIU**[††], ***Nonmembers***

SUMMARY To reduce the common mode voltage (CMV), suppress the CMV spikes, and improve the steady-state performance, a simplified reactive torque model predictive control (RT-MPC) for induction motors (IMs) is proposed. The proposed prediction model can effectively reduce the complexity of the control algorithm with the direct torque control (DTC) based voltage vector (VV) preselection approach. In addition, the proposed CMV suppression strategy can restrict the CMV within $\pm V_{dc}/6$, and does not require the exclusion of non-adjacent non-opposite VVs, thus resulting in the system showing good steady-state performance. The effectiveness of the proposed design has been tested and verified by the practical experiment. The proposed algorithm can reduce the execution time by an average of 26.33% compared to the major competitors.

key words: *induction motor, simplified reactive torque model predictive control, prediction model, common mode voltage, steady-state performance*

1. Introduction

Thanks to the advantages of simple structure, high reliability and easy maintenance, induction motors (IMs) have widely attracted widespread attention. As two basic closed-loop control algorithms of IMs, field-oriented control (FOC) and direct torque control (DTC) have attracted more attention [1]. In addition, model predictive control (MPC) has been widely studied and applied in the field of motor control due to its simplicity and fast closed-loop response in recent years [2], [3].

In the field of AC motor control, model predictive torque control (MPTC) has been paid special attention as it provides straightforward implementation, fast torque dynamic response, and the consideration of other constraints and nonlinearities [4]. The authors in [4]–[7] proposed the reactive torque MPC (RT-MPC) method to improve the system control including the model predictive current control (MPCC) and the model predictive flux control (MPFC). Also, the computational intensive control algorithm will affect the system performance in MPC. The existing computational burden reduction methods can generally be classified into two categories as reducing the complexity of prediction models and voltage vector (VV) preselection [5], [6], [8]–[11]. In [5] and [6], the torque and flux references are equivalently converted into a new flux reference or reference stator VV, thus reducing the complexity of prediction models.

The existing VV preselection methods can be divided into two categories as online calculation and lookup table (LUT) [8]–[11]. The candidate VVs are calculated based on the deadbeat principle for the online calculation method, which significantly reduces the computational burden and achieves better control performance [8]. LUT method includes different preselection methods by using DTC principle, deadbeat principle, and cost function [8]–[11].

In the two-level voltage source inverter (2L-VSI), the space vectors can be divided into two types, i.e., non-zero VV (NZVV) and zero VV (ZVV). Compared with NZVVs, the ZVV generates a higher common-mode voltage (CMV) amplitude, resulting in higher bearing current and shaft voltages, which causes damage to the motor and reduces the reliability of the overall motor drive system [12], [13]. Hardware-based and software-based solutions to suppress CMV have been widely used [14]–[25]. In the hardware-based method, filters and special topologies are the two main methods to suppress CMV, but this increases the hardware cost [14], [15]. In the software-based method, it can be divided into space vector pulse width modulation (PWM)-based method and MPC-based method [16]–[25].

MPC allows the consideration of other constraints and nonlinearities. Therefore, CMV can be suppressed by adding nonlinear or CMV terms with weighting factors to the cost function [17], [18]. Suppression of CMV by VV preselection is another MPC-based approach [19]–[26]. In [19]–[21], ZVV is abandoned, and only six NZVVs are adopted to restrict the CMV within $\pm V_{dc}/6$. In [20], a deadbeat control is proposed to reduce the candidate VVs. In [21], VV preselection considers both the reduction of switching loss and CMV. However, the effect of deadtime is not considered in [19]–[21]. In [22], it is pointed out that non-adjacent non-opposite NZVV switching combinations lead to CMV spikes. Therefore, all non-adjacent non-opposite NZVV switching combinations are pre-excluded. As a result, the CMV is completely restricted within $\pm V_{dc}/6$. In [23], the influence of deadtime on the non-adjacent non-opposite NZVV switching combination is analyzed, and the VV preselection method is further improved to improve the control performance. However, VV preselection methods that exclude non-adjacent non-opposite NZVV still have a negative effect on steady-state performance.

This paper proposes a simplified RT-MPC strategy with CMV suppression to reduce the CMV, suppress the CMV spikes, improve steady-state performance, and reduce the

Manuscript received August 7, 2023.
Manuscript revised October 20, 2023.
Manuscript publicized November 30, 2023.

[†]The authors are with College of Engineering Science and Technology, Shanghai Ocean University, Shanghai, 201306, China.
[††]The author is with School of Science, Engineering, and Technology, Penn State Harrisburg, Middletown PA 17057, USA.
a) E-mail: ycitwangbin@126.com

DOI: 10.1587/transele.2023ECP5034

computational burden. In order to reduce the computational burden, the DTC-based VV preselection method is used to reduce the number of candidate VVs, and a simplified prediction model is proposed. In addition, a novel CMV suppression strategy is proposed to restrict CMV within $\pm V_{dc}/6$. The proposed CMV suppression strategy does not need to exclude non-adjacent non-opposite NZVVs, thus resulting in good control performance. The rest of this paper is organized into four sections. Section 2 presents the theoretical basis of CMV and the classic RT-MPC. Section 3 presents the proposed simplified RT-MPC. The simulation and experimental validations are provided in Sect. 4, and the conclusion after the comparative study is given in Sect. 5.

2. Theoretical Basis of CMV and Traditional RT-MPC

2.1 Mathematical Model of IM

In the α-β coordinate system, the mathematical model of IM driven by a 2L-VSI is given by [7]

$$\boldsymbol{u}_s = R_s \boldsymbol{i}_s + \frac{d\boldsymbol{\psi}_s}{dt}, \tag{1}$$

$$\boldsymbol{\psi}_s = L_s \boldsymbol{i}_s + L_m \boldsymbol{i}_r = \boldsymbol{i}_s/(\lambda L_r) + L_m \boldsymbol{\psi}_r / L_r, \tag{2}$$

$$\boldsymbol{\psi}_r = L_m \boldsymbol{i}_s + L_r \boldsymbol{i}_r = -\boldsymbol{i}_s/(\lambda L_m) + L_r \boldsymbol{\psi}_s / L_m, \tag{3}$$

$$\boldsymbol{i}_s + \tau_\sigma \frac{d\boldsymbol{i}_s}{dt} = \frac{k_r}{R_\sigma}\left(\frac{1}{\tau_r} - jn_p\omega_m\right)\boldsymbol{\psi}_r + \frac{\boldsymbol{u}_s}{R_\sigma}, \tag{4}$$

where $\boldsymbol{u}_s = [\boldsymbol{u}_{s\alpha}\ \boldsymbol{u}_{s\beta}]^T$ is the stator VV; $\boldsymbol{i}_s = [\boldsymbol{i}_{s\alpha}\ \boldsymbol{i}_{s\beta}]^T$ and $\boldsymbol{i}_r = [\boldsymbol{i}_{r\alpha}\ \boldsymbol{i}_{r\beta}]^T$ are the stator and rotor current vector; $\boldsymbol{\psi}_s = [\boldsymbol{\psi}_{s\alpha}\ \boldsymbol{\psi}_{s\beta}]^T$ and $\boldsymbol{\psi}_r = [\boldsymbol{\psi}_{r\alpha}\ \boldsymbol{\psi}_{r\beta}]^T$ are the stator and rotor flux vector; R_s, L_s, L_r, L_m are the stator resistances, stator, rotor and mutual inductances, respectively; n_p and ω_m are the number of pole pairs and rotor angular speed, respectively; $\lambda = 1/(L_s L_r - L_m^2)$, $\tau_r = L_r/R_r$, $k_r = L_m/L_r$, $R_\sigma = R_s + R_r k_r^2$, $\tau_\sigma = \sigma L_s/R_\sigma$; $\sigma = 1 - L_m^2/(L_s L_r)$ is the leakage inductance coefficient; R_r is the rotor resistance.

2.2 Definition of CMV

The topology of IM fed by 2L-VSI is shown in Fig. 1 (a). The CMV is defined as the potential between the load neutral point and the center of the dc bus [19]. In Fig. 1 (a), the CMV can be calculated based on

$$U_{CMV} = \frac{u_{ao} + u_{bo} + u_{co}}{3} = \frac{V_{dc}}{6}(S_a + S_b + S_c), \tag{5}$$

where U_{CMV} and V_{dc} are the CMV of a 2L-VSI and the dc voltage, respectively; u_{xo} and $S_x (x \in \{a, b, c\})$ denote the voltage difference of phase x to o and the switching state of phase x, respectively. In addition, $S_x = 1$ represents the upper insulated-gate bipolar transistor (IGBT) of phase x is turned on, and the lower IGBT of phase x is turned on when $S_x = -1$.

According to equation (Eqn.) (6), the CMVs of eight VVs in Fig. 1 (b) can be calculated, as shown in Table I [19]. It can be seen that the CMV of NZVVs is $\pm V_{dc}/6$, while the ZVVs generate a larger absolute value of CMV.

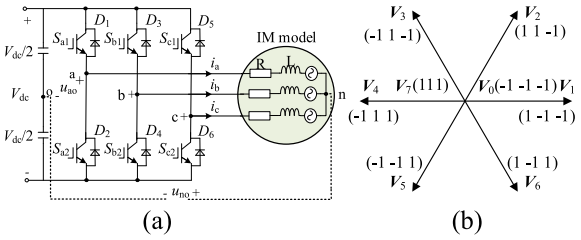

Fig. 1 IM system. (a) Topology of the system. (b) Eight VVs.

Table 1 CMV of different VVs

VVs		CMV
NZVVs	V_1, V_3, V_5	$-V_{dc}/6$
	V_2, V_4, V_6	$V_{dc}/6$
ZVVs	V_0	$-V_{dc}/2$
	V_7	$V_{dc}/2$

2.3 Effects of Dead Time

Nowadays, scholars have proposed some control strategies to suppress CMV, such as the six NZVVs (6VV) strategy [19]. Unfortunately, due to the deadtime effects, there are still some CMV spikes under switching between non-adjacent non-opposite NZVVs [22].

Thus, the five NZVVs (5VV) strategy is proposed in [22] to eliminate the deadtime effects. In 5VV method, the non-adjacent non-opposite NZVV switching combinations are abandoned to suppress CMV spikes. In addition, the ZVV is replaced with two opposite VVs to improve the steady-state performance. Therefore, the candidate VVs of 5VV strategy include one ZVV and four NZVVs. However, the torque, stator flux, and current total harmonic distortion (THD) of the 5VV strategy will be increased due to the non-adjacent non-opposite NZVVs are abandoned. In [23], the causes of equivalent ZVV under deadtime are analyzed in detail, the results show that the three-phase current direction and non-adjacent non-opposite NZVV switching combinations cause the CMV spikes. Therefore, a new VV preselection strategy is proposed. Compared to 5VV strategy, the steady-state performance has been improved.

2.4 Traditional RT-MPC

The control diagram of RT-MPC is shown in Fig. 2, $i_x (x \in \{a, b, c\})$ is the current of phase x, and $\boldsymbol{V}_{opt}$ is the optimal VV.

The external loop controller generates torque reference T_e^* and reactive torque reference T_R^* based on proportional-integral (PI), and the difference between reference speed ω_m^*, reference flux $|\boldsymbol{\psi}_s^*|$ and the corresponding actual speed and actual flux, respectively. For stator and rotor flux estimation, the basis state-space model of IM is given by

$$\begin{cases} \dfrac{\mathrm{d}\boldsymbol{i}_\mathrm{s}}{\mathrm{d}t} = A_1\boldsymbol{i}_\mathrm{s} + A_2\boldsymbol{\psi}_\mathrm{s} + B\boldsymbol{u}_\mathrm{s}, \\ \dfrac{\mathrm{d}\boldsymbol{\psi}_\mathrm{s}}{\mathrm{d}t} = A_3\boldsymbol{i}_\mathrm{s} + \boldsymbol{u}_\mathrm{s}, \end{cases} \tag{6}$$

$$\begin{cases} A_1 = jn_\mathrm{p}\omega_\mathrm{m} - \lambda(R_\mathrm{s}L_\mathrm{r} + R_\mathrm{r}L_\mathrm{s}), \\ A_2 = \lambda(R_\mathrm{r} - jL_\mathrm{r}n_\mathrm{p}\omega_\mathrm{m}),\ A_3 = -R_\mathrm{s},\ B = \lambda L_\mathrm{r}. \end{cases} \tag{7}$$

First, the Heun's method was used to discretize (6) to estimate the stator and rotor flux at k_th instant, and then to predict the parameters at $(k+1)_\mathrm{th}$ instant to compensate for the one-step delay in the digital implementation [5], [30].

Second, the stator flux and stator current at $(k+2)_\mathrm{th}$ instant under different candidate VVs are predicted according to the prediction model. Then, the reactive torque $T_\mathrm{R}(k+2)$ and torque $T_\mathrm{e}(k+2)$ under different VVs are obtained according to the predicted values [7]. The prediction model of RT-MPC is as follows

$$\boldsymbol{\psi}_\mathrm{s}(k+2) = \boldsymbol{\psi}_\mathrm{s}(k+1) + T_\mathrm{s}\boldsymbol{V}_i - R_\mathrm{s}T_\mathrm{s}\boldsymbol{i}_\mathrm{s}(k+1), \tag{8}$$

$$\begin{aligned} \boldsymbol{i}_\mathrm{s}(k+2) = {} & (k_\mathrm{r}(1 - jn_p\omega_\mathrm{m}\tau_\mathrm{r})\boldsymbol{\psi}_\mathrm{r}(k+1) + \tau_\mathrm{r}\boldsymbol{V}_i) \\ & T_\mathrm{s}/\tau_\sigma R_\sigma\tau_\mathrm{r} + (1 - T_\mathrm{s}/\tau_\sigma)\boldsymbol{i}_\mathrm{s}(k+1), \end{aligned} \tag{9}$$

$$T_\mathrm{e}(k+2) = 1.5n_\mathrm{p}\{\boldsymbol{\psi}_\mathrm{s}(k+2) \otimes \boldsymbol{i}_\mathrm{s}(k+2)\}, \tag{10}$$

$$T_\mathrm{R}(k+2) = 1.5n_\mathrm{p}\{\boldsymbol{\psi}_\mathrm{s}(k+2) \odot \boldsymbol{i}_\mathrm{s}(k+2)\}, \tag{11}$$

where $\boldsymbol{V}_i$ ($i \in \{0,1,2,\ldots,7\}$) represents the candidate VVs, $\otimes$ and $\odot$ are the external and inner product operators, respectively.

Third, a cost function containing reactive torque and torque is designed to evaluate the control performance of all candidate VVs, as shown in (12). It should be noted that since reactive torque and torque have the same dimension, the design of the weighting factors is avoided [7].

$$J = \left|T_\mathrm{e}^* - T_\mathrm{e}(k+2)\right| + \left|T_\mathrm{R}^* - T_\mathrm{R}(k+2)\right|, \tag{12}$$

where J represents the cost function value. The predicted of torque and reactive torque under different switching states are evaluated by (12), and the one that can minimize the cost function is chosen and applied during the next control cycle.

3. Proposed Simplified RT-MPC

3.1 Voltage Vectors Preselection

This paper uses the candidate VVs preselection method based on the DTC principle. The candidate VVs are selected using the present position of stator flux and torque deviation $\Delta T_\mathrm{e} = T_\mathrm{e}^* - T_\mathrm{e}$. The present position of stator flux θ is estimated as

$$\theta = \arctan(\psi_{\mathrm{s}\beta}(k+1)/\psi_{\mathrm{s}\alpha}(k+1)), \tag{13}$$

where $\psi_{\mathrm{s}\alpha}(k+1)$, $\psi_{\mathrm{s}\beta}(k+1)$ represents the real and imaginary parts of the stator flux $\psi_\mathrm{s}(k+1)$, respectively.

In 2L-VSI, the space distribution of all VVs in the α-β plane is divided into six sectors, and the sector number change periodically by an angle $\pi/3$ rad steps, as shown in Fig. 3. Thus, the relationship of the sector number N and the stator flux angle is given by

$$N = \mathrm{ceil}((3\theta + \pi/2)/\pi), \tag{14}$$

where ceil represents the function of rounding up.

As shown in Fig. 3, assuming $\boldsymbol{\psi}_\mathrm{s}(k+1)$ is located in sector I. For $\Delta T_\mathrm{e} > 0$, the VVs ($\boldsymbol{V}_2$, $\boldsymbol{V}_3$) satisfying torque increase (TI) are the candidate VVs. In addition, $\boldsymbol{V}_2$ and $\boldsymbol{V}_3$ also satisfied the possible condition of stator flux deviation $\Delta\psi_\mathrm{s} > 0$ or $\Delta\psi_\mathrm{s} < 0$, where $\Delta\psi_\mathrm{s} = |\boldsymbol{\psi}_\mathrm{s}^*| - |\boldsymbol{\psi}_\mathrm{s}|$, and $|\boldsymbol{\psi}_\mathrm{s}|$ is the amplitude of $\boldsymbol{\psi}_\mathrm{s}$. For $\Delta T_\mathrm{e} < 0$, $\boldsymbol{V}_5$ and $\boldsymbol{V}_6$ are the candidate VVs. When $\Delta T_\mathrm{e} = 0$, $\boldsymbol{V}_0$ is the candidate VV. Generally, it is necessary to employ the candidate VVs with the ZVV to reduce the torque and stator flux ripples. Hence, the total number of candidate VVs is three. With the same principle, the candidate VVs for all the sectors are shown in Table 2.

3.2 Simplified Prediction Model

In the traditional RT-MPC, the prediction model includes the prediction of stator flux, stator current, torque, and reactive torque, and the prediction of stator current is complicated and has a significant computational burden. Thus, an improved

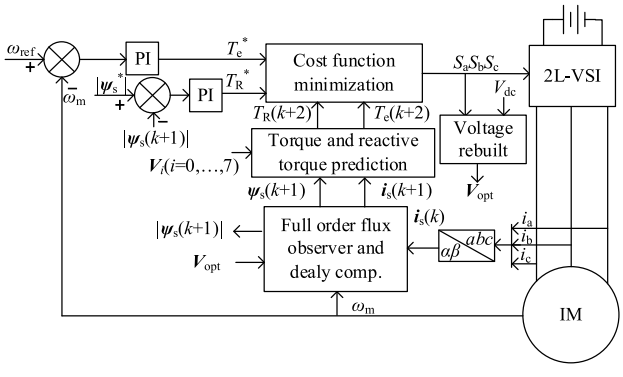

Fig. 2 Control diagram of RT-MPC.

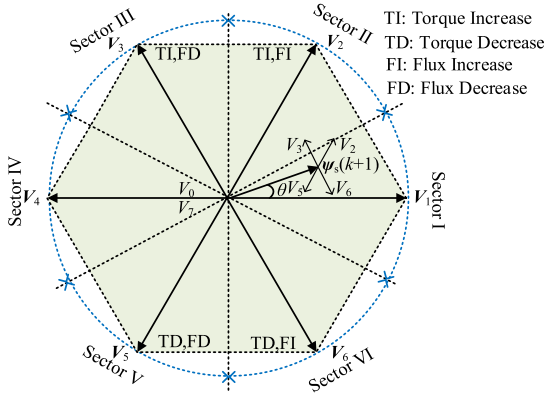

Fig. 3 Space distribution of all VVs of a 2L-VSI.

Table 2 Candidate VVs

	$\Delta T_e > 0$	$\Delta T_e < 0$	$\Delta T_e = 0$
Sector I	$V_2\ V_3\ V_0$	$V_5\ V_6\ V_0$	V_0
Sector II	$V_3\ V_4\ V_0$	$V_6\ V_1\ V_0$	V_0
Sector III	$V_4\ V_5\ V_0$	$V_1\ V_2\ V_0$	V_0
Sector IV	$V_5\ V_6\ V_0$	$V_2\ V_3\ V_0$	V_0
Sector V	$V_6\ V_1\ V_0$	$V_3\ V_4\ V_0$	V_0
Sector VI	$V_1\ V_2\ V_0$	$V_4\ V_5\ V_0$	V_0

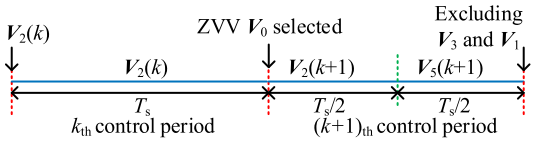

Fig. 4 Replacement method of ZVV proposed in [22].

prediction model is proposed in this paper to reduce the complexity of the prediction model.

Substituting (1) and (3) into (4) to eliminate the VV and the rotor flux term, the expression is as follows

$$\frac{\mathrm{d}\boldsymbol{i}_s}{\mathrm{d}t} = (jn_p\omega_m - \lambda R_r L_s)\boldsymbol{i}_s + \lambda L_r \frac{\mathrm{d}\boldsymbol{\psi}_s}{\mathrm{d}t} + \lambda(R_r - jL_r n_p \omega_m)\boldsymbol{\psi}_s, \tag{15}$$

According to first-order discretization, (15) can be shown as follows

$$\boldsymbol{i}_s(k+2) = \boldsymbol{i}_{sk} + \lambda L_r \boldsymbol{\psi}_s(k+2), \tag{16}$$

$$\boldsymbol{i}_{sk} = ((jn_p\omega_m - \lambda R_r L_s)\boldsymbol{i}_s(k+1) + \lambda(R_r - jL_r n_p \omega_m)\boldsymbol{\psi}_s(k+1))T_s + \boldsymbol{i}_s(k+1) - \lambda L_r \boldsymbol{\psi}_s(k+1). \tag{17}$$

According to (10) and (11), since $\boldsymbol{\psi}_s(k+2) \otimes \boldsymbol{\psi}_s(k+2) = 0$, $\boldsymbol{\psi}_s(k+2) \odot \boldsymbol{\psi}_s(k+2) = |\boldsymbol{\psi}_s(k+2)|^2$, the expressions of proposed prediction model for torque and reactive torque are demonstrated in Eqs. (18) and (19). Only the stator flux, torque, and reactive torque need to be predicted, which can effectively reduce the computational burden of the control algorithm.

$$T_e(k+2) = 1.5n_p\{\boldsymbol{\psi}_s(k+2) \otimes \boldsymbol{i}_{sk}\}, \tag{18}$$

$$T_R(k+2) = 1.5n_p\left\{\boldsymbol{\psi}_s(k+2) \odot \boldsymbol{i}_{sk} + \lambda L_r\left|\boldsymbol{\psi}_s(k+2)\right|^2\right\}. \tag{19}$$

3.3 CMV Reduction Strategy

Among the eight basic VVs generated by 2L-VSI, ZVV has a higher CMV. To reduce CMV, and ensure steady-state performance of IM, ZVV is often replaced with two NZVVs placed in opposite directions with respect to each other, as shown in Fig. 4. In addition, the non-adjacent non-opposite NZVV switching combinations should be abandoned to suppress CMV spikes at deadtime [22]. However, it has a negative influence on steady-state performance [23]. A novel CMV suppression strategy is proposed to improve the steady-state performance, reduce CMV and suppress CMV spikes. The CMV suppression strategy is as follows:

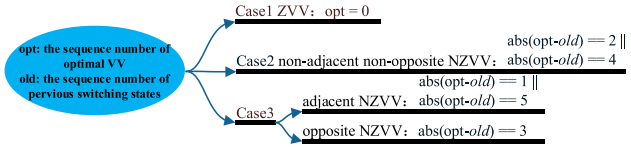

Fig. 5 Three types of optimal VVs.

Table 3 Switching sequences of different types of optimal VVs

	Condition	Switching sequence
Case 1	$old > 3$	$V_{old} - V_{(old-3)}$
	$old \le 3$	$V_{old} - V_{(old+3)}$
Case 2	$V_{opt} = V_x$	$V_y - V_x$
	$V_{opt} = V_y$	$V_x - V_y$
Case 3		V_{opt}

First, the optimal VV can be obtained from the three candidate VVs in Table 2, the simplified prediction model and the cost function of RT-MPC. Then, the optimal VV is divided into three categories according to the switching state of the previous control cycle: ZVV, non-adjacent non-opposite NZVV, and adjacent or opposite NZVV. The principle of distinction is shown in Fig. 5, opt and old are the subscript i of VV V_i.

Second, it is processed according to different types of optimal VVs, for the ZVV of case 1, utilizing the switching sequence shown in Fig. 4. When it is an opposite or adjacent NZVV of case 3, the optimal VV is used as the output in one control cycle. For the optimal VV in case 2, discarding the optimal VV may result in a poor steady-state performance but will produce CMV spikes during application. Therefore, a control strategy is proposed to suppress CMV spikes and improve steady-state performance.

The proposed control strategy inserts intermediate VV between non-adjacent non-opposite NZVVs. For example, assuming that the optimal VV at the previous control cycle is V_2. In the present cycle, V_0, V_3, and V_4 are the candidate VVs, and V_4 is the optimal VV. Therefore, V_3 is inserted between V_2 and V_4. Thus, the optimal VV of the present control cycle consists of V_3 and V_4. The duty cycle of V_3 can be a fixed value or obtained by using duty cycle calculation methods such as modulation MPC [27]–[29]. In this case, the steady-state performance of the controller is improved while the CMV is suppressed. The proposed CMV reduction strategy is summarized in Table 3, V_{old}, V_{opt}, V_y, V_x are the previous, present control cycle optimal VV and the two candidate NZVVs, respectively.

3.4 Proposed Control Flow

The control diagram of the simplified RT-MPC method is shown in Fig. 6. For clarity, the control flow is summarized in the following steps:

Step 1: Measurement: sample the three-phase current and rotor speed, then calculate the stator current in α-β frame.

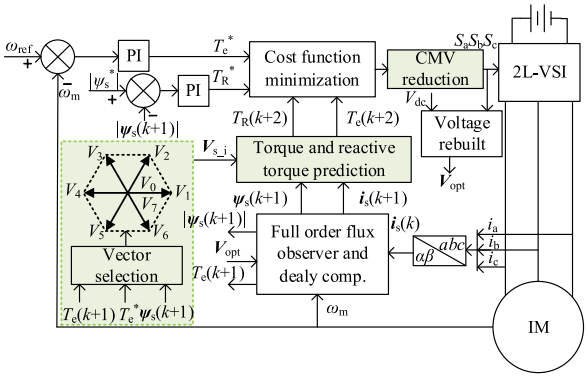

Fig. 6 Control diagram of the simplified RT-MPC.

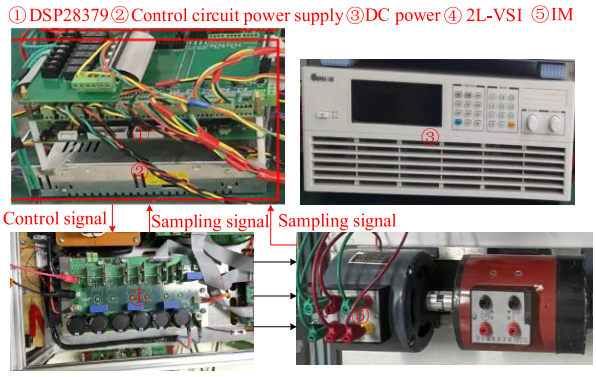

Fig. 7 IM experiment platform.

Step 2: Apply: apply the optimal VV $\boldsymbol{V}_{\text{opt}}$ of the previous control cycle.

Step 3: Estimate and delay compensation: estimate stator and rotor flux respectively. Then, predict stator current, stator, and rotor flux based on $\boldsymbol{V}_{\text{opt}}$.

Step 4: VV preselection: candidate VVs are selected according to (13), (14), torque deviation, and Table 2.

Step 5: Prediction: stator flux, torque, and reactive torque, are predicted by (8), (18), (19).

Step 6: Cost function evaluation: the cost function (12) is used to evaluate the predicted torque and reactive torque values, and the optimal closed-loop action is obtained.

Step 7: CMV reduction: the optimal VV is classified according to Fig. 5, then the switching sequence is obtained according to Table 3.

4. Experimental Verification and Result Analysis

A test bench of the IM control system is established to verify the validity of the proposed simplified RT-MPC strategy, as shown in Fig. 7. The algorithm uses DSP28379D as the core control device on the experimental platform. The IM uses a 4-pole motor with a rated voltage 380 V, rated power 1.5 kW, and rated shaft speed 1400 r/min; the parameters of IM are listed in Table 4. The IM is driven by IGBT module (SKM50GB123D), and the DC bus voltage is about 540 V. The RT-MPC [8], 6VV strategy [19], 5VV strategy [22], and the proposed simplified RT-MPC are evaluated under 20 kHz operating conditions. In addition, the duty cycle of the inserted VV in case 2 of simplified RT-MPC is 0.5. It is noted that only the simplified RT-MPC uses the simplified prediction model, while other methods use the prediction model in reference [7].

4.1 Execution Time Comparison

The execution time of four control strategies is shown in Fig. 8. The execution time of cost function optimization depends on the number of candidate VVs and the complexity of the prediction model, which is the most important to the overall execution time. RT-MPC, 6VV strategy, 5VV strategy, and simplified RT-MPC rely on 7, 6, 5, and 3 iterations

Table 4 IM parameters

Variables	Parameters	Values
U_{N}	Rated voltage	380 V
n_{p}	Number of pole pairs	2
R_{s}	Stator resistance	2.742 Ω
R_{r}	Rotor resistance	1.08 Ω
L_{m}	Mutual inductance	0.2498 H
L_{s}	Stator inductance	0.2582 H
L_{r}	Rotor inductance	0.2582 H
$\lvert\psi_{\text{s}}^*\rvert$	Flux amplitude reference	0.82 Wb

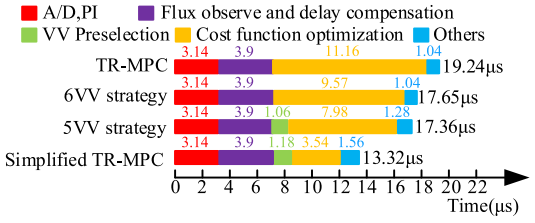

Fig. 8 Execution time of four control strategies.

respectively, and the simplified prediction model reduces the execution time of a single prediction. As a result, compared with RT-MPC, 6VV strategy and 5VV strategy, the execution time of the proposed simplified RT-MPC was reduced by approximately 31%, 25%, and 23%, respectively. An average of 26.33% performance improvement is reached based on the proposed control model.

4.2 Control Performance Comparison

The steady-state performance of RT-MPC, 6VV strategy, 5VV strategy, and simplified RT-MPC under different conditions are tested, as shown in Figs. 9, 10 and 11. In Figs. 9, 10 and 11, the IM operates at 200 r/min, 800 r/min, and 1400 r/min with 10 Nm load, respectively. From top to bottom are stator flux, torque, stator current, and the amplitude of CMV. In order to quantitatively evaluate the steady-state performance of four control strategies, the torque and stator flux ripple $T_{\text{e\_ripple}}$, $\psi_{\text{s\_ripple}}$ are as follows

$$T_{\text{e\_ripple}} = \sqrt{\frac{1}{n}\sum_{x=1}^{n}(T_{\text{e}}(x) - T_{\text{e}}^*)^2}, \tag{20}$$

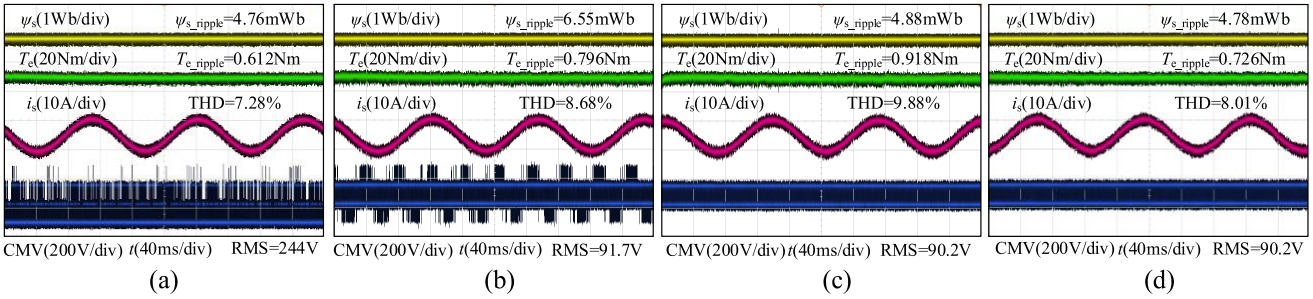

Fig. 9 Steady-state performance comparison under 200 r/min, 10 Nm load. (a) RT-MPC. (b) 6VV strategy. (c) 5VV strategy. (d) Simplified RT-MPC.

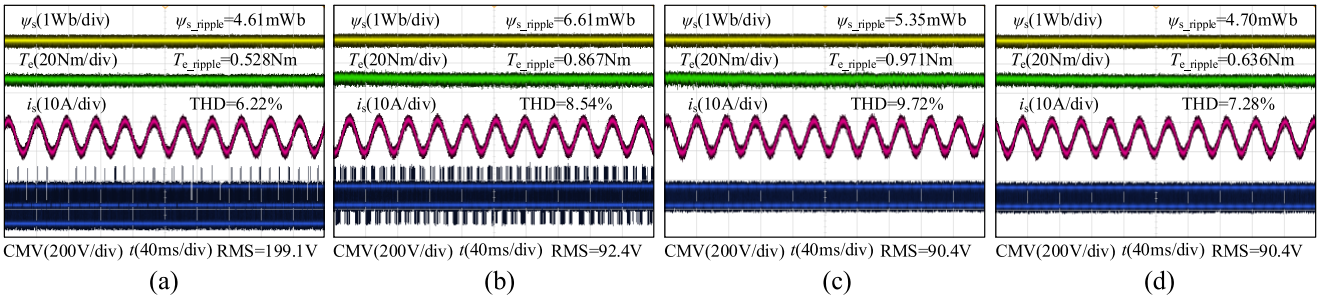

Fig. 10 Steady-state performance comparison under 800 r/min, 10 Nm load. (a) RT-MPC. (b) 6VV strategy. (c) 5VV strategy. (d) Simplified RT-MPC.

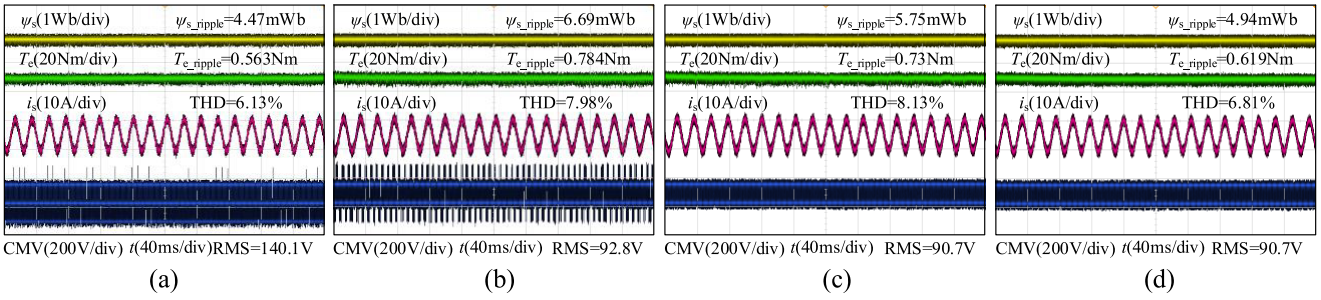

Fig. 11 Steady-state performance comparison under 1400 r/min, 10 Nm load. (a) RT-MPC. (b) 6VV strategy. (c) 5VV strategy. (d) Simplified RT-MPC.

$$\psi_{\text{s\_ripple}} = \sqrt{\frac{1}{n}\sum_{x=1}^{n}(\psi_{\text{s}}(x) - |\psi_{\text{s}}^{*}|)^2}, \tag{21}$$

where $T_{\text{e}}(x)$ and $\psi_{\text{s}}(x)$ are the measured torque and stator flux, respectively, and n represents the number of samplings.

As shown in Figs. 9 (a), 10 (a), and 11 (a), RT-MPC uses 6 NZVVs and 1 ZVV, thus the flux, torque ripple, and current THD are lowest, and CMV root mean square (rms) values is highest among the four control strategies. The CMV rms values under different speeds are 244 V,199.1 V, and 140.1 V respectively. When the rotor speed increases, the frequency of NZVV as the optimal VV increases, resulting in the CMV rms decreases. In addition, ZVV $\boldsymbol{V}_0$ and deadtime effects result in CMV with an amplitude of $\pm V_{\text{dc}}/2$ [22]. In the 6VV strategy in Figs. 9 (b), 10 (b), and 11 (b), the steady-state performance is decreased due to ZVV elimination. In addition, the effect of deadtime results in CMV spikes with an amplitude of $\pm V_{\text{dc}}/2$, and the CMV rms values are 91.7 V, 92.4 V, and 92.8 V.

Unlike the RT-MPC and 6VV strategies, the CMV of 5VV and simplified RT-MPC strategies can be restricted to $\pm V_{\text{dc}}/6$, as shown in Figs. 9 (c), (d), Figs. 10 (c), (d), and Figs. 11 (c), (d). The CMV rms values of both methods are about 90 V. The experimental results verify that the proposed simplified RT-MPC can effectively reduce CMV and eliminate CMV spikes caused by deadtime effect. The flux, torque ripple and current THD of four control strategies at different speeds are shown in Figs. 12 (a), (b), and (c). In the VV preselection stage, the 6VV strategy directly excludes ZVV, and the 5VV strategy excludes non-adjacent non-opposite NZVV switching combinations, thus deteriorating steady-state performance. As shown in Fig. 12, the stator flux, torque ripple, and current THD of simplified RT-MPC are better than those of 6VV and 5VV strategies.

Therefore, the simplified RT-MPC effectively reduces the CMV, suppress CMV spikes, and provide better steady-state performance.

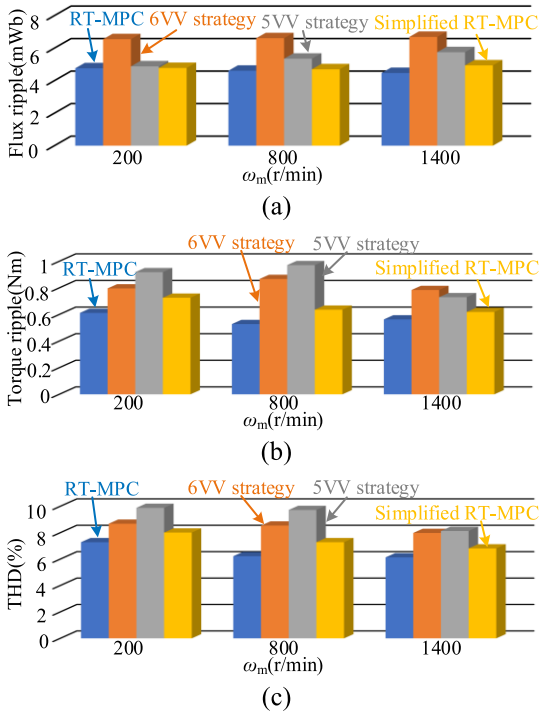

Fig. 12 Rms of different indicators. (a) Flux. (b) Toque. (c) THD.

The dynamic performance of the four control strategies is tested. Figure 13 presents the dynamic response results when the reference speed changes from 1400 r/min to −1400 r/min, and the dynamic response results of external load disturbance under rated speed are shown in Fig. 14. Although the four control strategies have different VV preselection principles, they have almost the similar dynamic response, which indicates that the proposed method can still have good dynamic performance after reducing the candidate VVs. Figure 13 also shows that the simplified RT-MPC method has good control performance under fast-speed step change. In addition, the CMV of 5VV and simplified RT-MPC strategies can be restricted to $\pm V_{dc}/6$ under rated speed reversal and an external load disturbance, as shown in Figs. 13 (c), (d), and Figs. 14 (c), (d). The above experimental results also show that the simplified prediction model has almost no negative effect on the RT-MPC algorithm.

4.3 Parameter Sensitivity Experiment

In order to validate the robustness against motor parameter deviation based on the simplified RT-MPC method, the stator, rotor resistance, and inductance mismatch waveforms are shown in Figs. 15 (a), (b), (c), and (d), respectively. R_s, R_r, L_s, and L_r are the parameters of stator, rotor resistance, and inductance in the control algorithm respectively. Compared with the rotor side parameter mismatch, the stator side parameter mismatch has more influence on the steady-state performance. The stator current and torque increase

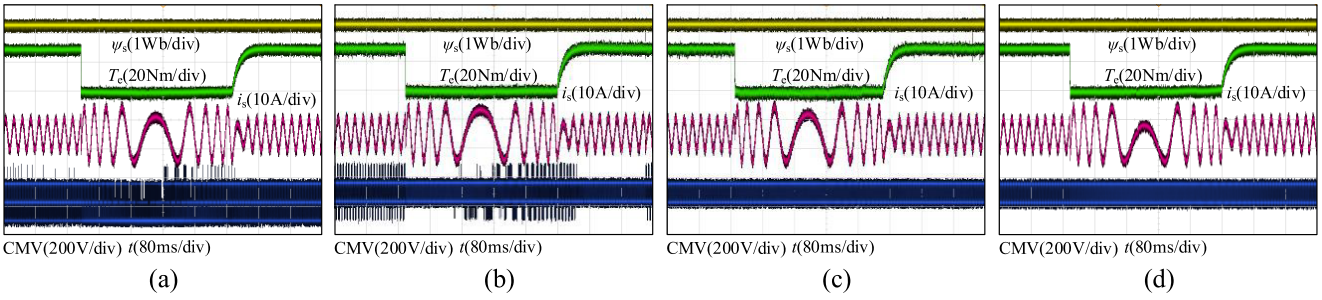

Fig. 13 Rated speed reversal condition comparison. (a) RT-MPC. (b) 6VV strategy. (c) 5VV strategy. (d) Simplified RT-MPC.

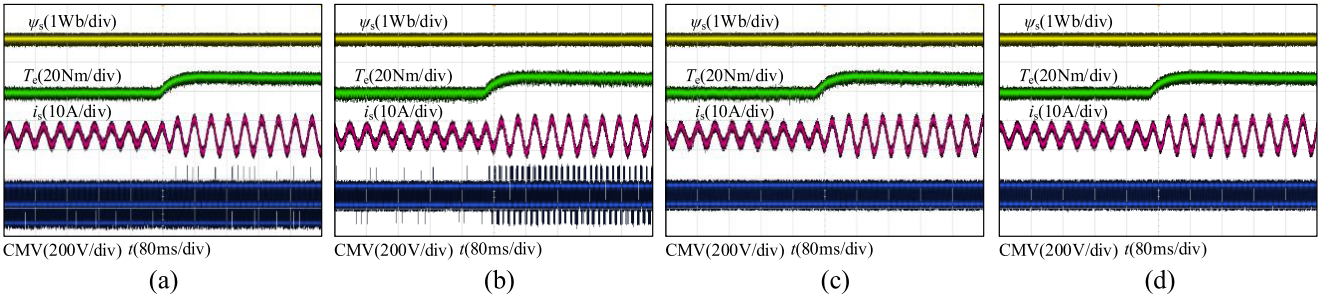

Fig. 14 External load disturbance under rated speed. (a) RT-MPC. (b) 6VV strategy. (c) 5VV strategy. (d) Simplified RT-MPC.

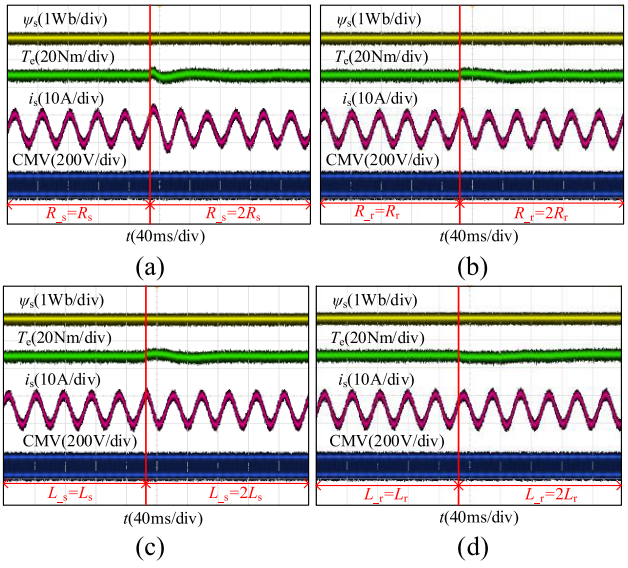

Fig. 15 Experimental waveforms of robustness against parameter sensitivity of simplified RT-MPC. (a) R_s. (b) R_r. (c) L_s. (d) L_r.

with the increase of the stator resistance, after a transient process for a period of time, and then return to a steady state. When the stator inductance is increased, the stator current and torque return to the steady state after a short transient process. When the parameters on the rotor side are mismatched, there is almost no negative effect on steady-state performance. In addition, the CMV of the simplified RT-MPC strategy can be restricted to $\pm V_{dc}/6$ under IM parameters mismatch.

5. Conclusion

In this paper, a new simplified RT-MPC strategy is proposed to reduce CMV, torque, stator flux ripple, current THD, and suppress CMV spikes. To reduce the execution time of proposed method, the DTC-based VV preselection method and a novel simplified prediction model are used to reduce the complexity of RT-MPC strategy. The experimental results show that the simplified prediction model has no negative effect on RT-MPC algorithm. In addition, a new CMV suppression strategy considering deadtime effects is proposed to restrict the CMV spikes and improve the steady-state performance. The experimental results show that compared to the RT-MPC and 6VV strategy, the simplified RT-MPC can restrict CMV within $\pm V_{dc}/6$ and reduce execution time. Compared to 5VV strategy, the simplified RT-MPC has better steady-state performance and lower execution time. In addition, the experimental results also show that simplified RT-MPC has good parameters robustness.

Acknowledgements

This work was supported in part by Shanghai Municipal Science and Technology Commission of China (Grant No.19DZ2254800), and by Shanghai Science and Technology Innovation Action Plan (No.21DZ1205500).

References

[1] D. Casadei, F. Profumo, G. Serra, and A. Tani, "FOC and DTC: two viable schemes for induction motors torque control," IEEE Trans. Power Electron., vol.17, no.5, pp.779–787, Sept. 2002.
[2] H. Zhou, L. Kang, X. Duan, M. Zhao, "Secondary ripple suppression Strategy for a single-phase PWM rectifier based on constant frequency current predictive control," IEICE Trans. Electron., vol.E105-C, no.11, pp.667–674, Nov. 2022.
[3] S. Vazquez, J. Rodriguez, M. Rivera, L.G. Franquelo, and M. Norambuena, "Model predictive control for power converters and drives: advances and trends," IEEE Trans. Ind. Electron., vol.64, no.2, pp.935–947, Feb. 2017.
[4] F. Wang, S. Li, X. Mei, W. Xie, J. Rodríguez and R.M. Kennel, "Model-based predictive direct control strategies for electrical drives: an experimental evaluation of PTC and PCC methods," IEEE Trans. Ind. Informat., vol.11, no.3, pp.671–681, June 2015.
[5] T. Jin, H. Song, P.G. Ipoum-Ngome, D.L. Mon-Nzongo, J. Tang, M. Zhu, and J. Rodriguez, "Low complexity model predictive flux control based on discrete space vector modulation and optimal switching sequence for induction motors," IEEE Trans. Ind. Electron., vol.71, no.1, pp.305–315, Jan. 2024.
[6] X. Zhang and B. Hou, "Double vectors model predictive torque control without weighting factor based on voltage tracking error," IEEE Trans. Power Electron., vol.33, no.3, pp.2368–2380, March 2018.
[7] Z. Lu, R. Zhang, L. Hu, L. Gan, J. Lin, and P. Gong, "Model predictive control of induction motor based on amplitude-phase motion equation," IET Power Electron., vol.12, no.9, pp.2400–2406, Aug. 2019.
[8] T. Jin, H. Song, D.L. Mon-Nzongo, P.G. Ipoum-Ngome, H. Liao, and M. Zhu, "Virtual three-level model predictive flux control with reduced computational burden and switching frequency for induction motors," IEEE Trans. Power Electron., vol.38, no.2, pp.1571–1582, Feb. 2023.
[9] M. Amiri, J. Milimonfared, and D.A. Khaburi, "Predictive torque control implementation for induction motors based on disc rete space vector modulation," IEEE Trans. Ind. Electron., vol.65, no.9, pp.6881–6889, Sept. 2018.
[10] I.M. Alsofyani and K.-B. Lee, "A unidirectional voltage vector preselection strategy for optimizing model predictive torque control with discrete space vector modulation of IPMSM," IEEE Trans. Ind. Electron., vol.69, no.12, pp.12305–12315, Dec. 2022.
[11] I. Osman, D. Xiao, K.S. Alam, S.M.S.I. Shakib, M.P. Akter, and M.F. Rahman, "Discrete space vector modulation-based model predictive torque control with no suboptimization," IEEE Trans. Ind. Electron., vol.67, no.10, pp.8164–8174, Oct. 2020.
[12] J.M. Erdman, R.J. Kerkman, D.W. Schlegel, and G.L. Skibinski, "Effect of PWM inverters on ac motor bearing currents and shaft voltages," IEEE Trans. Ind. Appl., vol.32, no.2, pp.250–259, March-April 1996.
[13] X. Guo, Y. Yang, and T. Zhu, "ESI: a novel three-phase inverter with leakage current attenuation for transformerless PV systems," IEEE Trans. Ind. Electron., vol.65, no.4, pp.2967–2974, April 2018.
[14] K. Kang, K.-Y. Jung, and S.W. Nam, "Passive-filter-configuration-based reduction of up-to-several-hundred-MHz EMI noises in H-Bridge PWM micro-Stepping motor driver circuits," IEICE Trans. Electron., vol.E101-C, no.2, pp.104–111, Feb. 2018.
[15] A. Hota and V. Agarwal, "Novel three-phase H10 inverter topology with zero or constant common-mode voltage for three-phase induction motor drive applications," IEEE Trans. Ind. Electron., vol.69, no.7, pp.7522–7525, July 2022.
[16] K. Tian, J. Wang, B. Wu, Z. Cheng, and N.R. Zargari, "A virtual space vector modulation technique for the reduction of common-mode voltages in both magnitude and third-order component," IEEE

Trans. Power Electron., vol.31, no.1, pp.839–848, Jan. 2016.
[17] M.J. Duran, J.A. Riveros, F. Barrero, H. Guzman, and J. Prieto, "Reduction of common-mode voltage in five-phase induction motor drives using predictive control techniques," IEEE Trans. Ind. Appl., vol.48, no.6, pp.2059–2067, Nov.-Dec. 2012.
[18] X. Wang, X. Fang, S. Lin, F. Lin, and Z. Yang, "Predictive common-mode voltage suppression method based on current ripple for permanent magnet synchronous motors," IEEE Trans. Emerg. Sel. Topics Power Electron., vol.7, no.2, pp.946–955, June 2019.
[19] S.K. Hoseini, J. Adabi, and A. Sheikholeslami, "Predictive modulation schemes to reduce common-mode voltage in three-phase inverters-fed ac drive systems," IET Power Electron., vol.7, no.4, pp.840–849, April 2014.
[20] S.-K. Mun and S. Kwak, "Reducing common-mode voltage of three-phase VSIs using the predictive current control method based on reference voltage," J. Power Electron., vol.15, no.3, pp.712–720, May 2015.
[21] L. Guo, X. Zhang, S. Yang, Z. Xie, and R. Cao, "A model predictive control-based common-mode voltage suppression strategy for voltage source inverter," IEEE Trans. Ind. Electron., vol.63, no.10, pp.6115–6125, Oct. 2016.
[22] S. Kwak and S. Mun, "Common-mode voltage mitigation with a predictive control method considering dead time effects of three-phase voltage source inverters," IET Power Electron., vol.8, no.9, pp.1690–1700, Sept. 2015.
[23] L. Guo, N. Jin, C. Gan, L. Xu, and Q. Wang, "An improved model predictive control strategy to reduce common-mode voltage for two-level voltage source inverters considering dead-time effects," IEEE Trans. Ind. Electron., vol.66, no.5, pp.3561–3572, May 2019.
[24] S. Kwak and S.-K. Mun, "Model predictive control methods to reduce common-mode voltage for three-phase voltage source inverters," IEEE Trans. on Power Electron., vol.30, no.9, pp.5019–5035, Sept. 2015.
[25] L. Guo, N. Jin, C. Gan, and K. Luo, "Hybrid voltage vector preselection-based model predictive control for two-level voltage source inverters to reduce the common-mode voltage," IEEE Trans. Ind. Electron., vol.67, no.6, pp.4680–4691, June 2020.
[26] J. Li, W. Song, B. Liu, B. Yu, and J. Feng, "Model predictive pulse pattern control of permanent magnet synchronous motor with low torque ripple and common mode voltage," Proc. CSEE, vol.42, no.11, pp.4189–4199, Jan. 2022.
[27] J. Xu, T.B. Soeiro, F. Gao, L. Chen, H. Tang, P. Bauer, and T. Dragicevic, "Carrier-based modulated model predictive control strategy for three-phase two-level VSIs," IEEE Trans. Energy Convers., vol.36, no.3, pp.1673–1687, Sept. 2021.
[28] . Jin, Q. Xiao, H. Jia, Y. Mu, Y. Ji, T. Dragieevic, R. Teodorescu, and F. Blaabjerg, "A novel sliding-discrete-control-set modulated model predictive control for modular multilevel converter," IEEE Access, vol. 9, pp.10316–10327, 2021.
[29] X. Li, T. Peng, H. Dan, G. Zhang, W. Tang, W. Jin, P. Wheeler, and M. Rivera, "A modulated model predictive control scheme for the brushless doubly fed induction machine," IEEE J. Emerg. Sel. Topics Power Electron., vol.6, no.4, pp.1681–1691, Dec. 2018.
[30] P. Cortes, J. Rodriguez, C. Silva, and A. Flores, "Delay compensation in model predictive current control of a three-phase inverter," IEEE Trans. Ind. Electron., vol.59, no.2, pp.1323–1325, Feb. 2012.

Siyao Chu received his bachelor's degree in electrical engineering from Qingdao University of Technology in China in 2017 and is now pursuing a master's degree at Shanghai Ocean University.

Bin Wang is, 2019–present, Professor, School of Engineering, Shanghai Ocean University. 1998–2019, Yancheng Institute of Technology, School of Mechanical Engineering, Lecturer, Associate Professor, Professor. 2016–2017, Pennsylvania State University, visiting scholar. 2009–2015, Tongji University, School of Automotive Engineering, Vehicle Engineering, Ph.D. 2003–2006, Guizhou University, School of Mechanical Engineering, Master of Mechanical Design Theory. 1994–1998, Xi'an Jiaotong University, School of Mechanical Engineering, Bachelor of Mechanical Engineering.

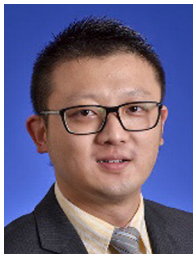

Xinwei Niu received his B.S. degree from Xi'an University of Architecture and Technology, China (2005), M.S. degree from Northwestern Polytechnical University, China (2008), and Ph.D. degree from Florida International University (2013). He is currently an assistant professor in the Electrical Engineering department at Penn State Harrisburg. His research interests are in the areas of database system management, high performance computing, and hardware acceleration.